

EFDA–JET–CP(12)02/29

D. Tskhakaya, M. Groth
and JET EFDA contributors

1D Kinetic Modelling of the JET SOL with Tungsten Divertor Plates

“This document is intended for publication in the open literature. It is made available on the understanding that it may not be further circulated and extracts or references may not be published prior to publication of the original when applicable, or without the consent of the Publications Officer, EFDA, Culham Science Centre, Abingdon, Oxon, OX14 3DB, UK.”

“Enquiries about Copyright and reproduction should be addressed to the Publications Officer, EFDA, Culham Science Centre, Abingdon, Oxon, OX14 3DB, UK.”

The contents of this preprint and all other JET EFDA Preprints and Conference Papers are available to view online free at www.iop.org/Jet. This site has full search facilities and e-mail alert options. The diagrams contained within the PDFs on this site are hyperlinked from the year 1996 onwards.

1D Kinetic Modelling of the JET SOL with Tungsten Divertor Plates

D. Tskhakaya, M. Groth
and JET EFDA contributors*

JET-EFDA, Culham Science Centre, OX14 3DB, Abingdon, UK

¹*Association EURATOM-ÖAW, University of Innsbruck, A-6020 Innsbruck, Austria*

²*Aalto University, Association EURATOM-Tekes, Otakaari 4, 02015 Espoo, Finland*

^c*Permanent address: Andronikashvili Institute of Physics, 0177 Tbilisi, Georgia*

** See annex of F. Romanelli et al, "Overview of JET Results",
(23rd IAEA Fusion Energy Conference, Daejeon, Republic of Korea (2010)).*

Preprint of Paper to be submitted for publication in Proceedings of the
20th International Conference on Plasma Surface Interactions , Eurogress, Aachen, Germany
21st May 2012 - 25th May 2012

ABSTRACT

In this work a fully kinetic model of the JET SOL with tungsten divertor plates has been developed. It includes the dynamics of main-ions (D+) and electrons, the neutrals (D, C, W) and the impurity particles (C^{+m} , W^{+n}). Our simulations show extremely low concentration of W impurity. We identify two reasons which are responsible for this effect: 1. for low temperature divertor plasma the energy of most of the main-ions and the impurities in a low-ionization state impinging the divertor plates is below the W-sputtering threshold energy; 2. with increasing temperature the W-sputtering increases, but the potential drop across the divertor plasma increases too, so that most of the W ions are reabsorbed at the divertors.

1. INTRODUCTION

Tungsten is becoming a common divertor material for our day and future tokamaks. As a result, the development of the corresponding SOL models has become one of most important topics in fusion plasma research. In the present work we model tungsten generation and transport along the field lines in the JET SOL using fully kinetic approach: the plasma (e, D⁺), the neutral (D, C, W) and the impurity (W^{+n} , C^{+m}) particles are treated kinetically.

The simulations of this type are extremely CPU-intensive. There are several reasons for using such modeling. It has been demonstrated that kinetic effects can dominate in the high recycling plasma even if there are only common impurities like carbon (see[1–5] and references their). Introduction of massive high-z impurities complicates the problem, so that the kinetic effects can become essential. Here we mention two additional effects.

First of all, massive high-Z impurities (like tungsten) can not be treated as trace impurities. E.g. the friction force between different ionized states of W, $R_{W^{+k}W^{+n}}$, can be of the same order as the friction force between W and main D ions, $R_{W^{+k}D^+}$, [6]:

$$\sum_{n \neq k} R_{W^{+k}W^{+n}} / R_{W^{+k}D^+} \sim \sqrt{M_W / M_D} \approx 10 \sum_{n \neq k} n^2 c_{W^{+n}}, \quad (1)$$

where, $M_{W,D}$, are particle masses and $c_{W^{+n}}$ is the W^{+n} concentration. As we see, if $\sum_{n \neq k} n^2 c_{W^{+n}} \sim 0.1$, then the friction force between W ions can not be neglected. We note that due to lower mass ratio this effect is practically negligible for light impurities.

The second effect is related to the tungsten sputtering, which is strongly coupled with the divertor plasma parameters and extremely sensitive to the energy of ions impinging at the divertor plates. It is usually assumed that this ions are accelerated in a constant (in time) sheath potential drop $\sim 3T_e / (T_e$ is the electron temperature). In reality the potential oscillates around this average value, which may accelerate resonant ions up to energies more than $3T_e$. In Fig.1 is plotted the oscillation spectrum of the potential at the magnetic presheath entrance in the outer divertor plasma (the divertor potential is set to zero). The maximum at low frequency is near to C^+ cyclotron and the other two correspond to the lower and upper hybrid wave frequencies [7]:

$$\omega_{LH,UH} = \left[\frac{\Omega_e^2 + \omega_p^2}{2} \pm \sqrt{\frac{(\Omega_e^2 + \omega_p^2)^2}{4} - \omega_p^2 \Omega_e^2 \sin^2 \theta} \right]^{1/2}, \quad (2)$$

where, Ω_e and ω_p the electron cyclotron and plasma frequencies; θ is the angle between the magnetic field and the divertor surface. Although the amplitude of these oscillations is lower than the average potential ($\sim 110\text{eV}$), it is not obvious that the additional energy gain by resonant ions is negligible. Moreover, the tungsten atoms can be ionized near to the divertor plates and the probability to return back to the plates strongly depends on the electric field (and its oscillations) in the sheath. As we will see below, exactly this redeposition is responsible for significant reduction of the effective W-sputtering yield.

These examples indicate that for realistic self-consistent modelling of the W generation and transport in the SOL a fully kinetic approach is required.

2. DESCRIPTION OF THE SOL MODEL

For the simulation we have updated the original Particle in Cell (PIC) Monte Carlo (MC) code “BIT1” by including new physics and optimization of number of numerical routines. BIT1 is a quasi-2D massively parallel kinetic code for simulation of the SOL [8]. The simulation geometry represents a rectangular box two sides which correspond to the divertor plates and the other two to the separatrix and to the outer wall (see Fig.2). The plasma, the neutral and the impurity particles are treated in 1D3V, 2D3V and quasi-2D3V approximation, respectively (nDmV means n-dimensional in usual and m-dimensional in velocity space). Hot (120-250eV) plasma (e, D^+), impurity (C^{++}) and heat source correspond to the particle and heat transport across the separatrix. After the injection plasma and impurity particles propagate along the magnetic field towards the divertor. The particle absorbed at the divertor plates cause injection of secondary particles (secondary electrons, D, C and W atoms). These atoms interact with the plasma in a nonlinear way. Atoms reaching the radial boundaries of the system (i.e. the separatrix and the outer wall) are removed from the system. Impurity ions, C^{+m} , W^{+n} , are also removed from the simulation with the probability corresponding to the anomalous cross-field diffusion coefficient $D_{\perp} \sim 1 \text{ m}^2/\text{s}$ and cross-field gradient length $\sim 1\text{cm}$. To keep quasineutrality the corresponding number of electrons is removed together with the impurity ions. The strength of the particle and heat sources and the temperature of the incoming particles are adjusted to match the experimentally observed plasma density and electron temperature in the upstream SOL. For other details of the simulation see [1, 5].

All the collision operators used in the code are nonlinear and conserve the particle number, the momentum and the energy. The number of simulated particle species is limited (practically) by available atomic and PSI (Plasma-Surface Interaction) data. In the given simulations we included C^{+m} , W^{+n} , $m = 0, \dots, 2$, $n = 0, \dots, 11$, impurity ions, hence together with electrons and the main ions there 15 different types of charged particles interacting with each other. In the simulations we do not observe highly ionized tungsten ions ($n > 4$), so that the number collision types is reduced significantly.

The threshold energy for W sputtering due to D impact is too low to produce any reasonable amount of W [9, 10] (our test simulations also confirm this). In realistic plasmas, light impurities, like C and Be having relatively low W-sputtering threshold energies, are the catalysts for W production. Both C and Be have comparable mass and threshold energies, and may be equally used in the simulations for production of W. In order to simplify the model we consider only C impurities. The original BIT1 included all necessary atomic and PSI processes for simulation of e, D⁺, C^{+m} plasmas. Hence, the only missing part was the tungsten-related atomic and PSI processes.

2.1. IMPLEMENTATION OF ATOMIC PROCESSES

For the atomic processes in the BIT1 code we consider single and double electron-impact ionizations of W⁺ⁿ, for n < 11 and n < 7, respectively. The corresponding cross-sections are taken from [11, 12]. Some of cross-sections are given for energies below 1keV. In this case we extrapolated the cross-sections according to the expression:

$$\sigma = \frac{A \ln(E) + B}{E}. \quad (3)$$

The obtained cross-sections are plotted in Fig.3. The after-collision electrons are assumed to be isotropically scattered.

2.2. IMPLEMENTATION OF PSI PROCESSES.

Contrary to the ionization-cross sections there is a large spread in tungsten-related PSI data. E.g. the tungsten self-sputtering yield given in [9] is too large and results, according to our test simulations, in unphysically high W concentration ($\sim 0.5 \times 10^{20} \text{ m}^{-2}$). Eckstein in [10] proposes more realistic sputtering yields (see Fig.4), which are implemented in the BIT1. Unfortunately, in [10] the W sputtering yields due to carbon impact are missing, hence we used the data from [9] with the corrected threshold energy (45eV) considered in [13].

The probability that after ionization the sputtered W returns back to the divertor strongly depends on the distribution of sputtered W atoms. Hence, we implemented the following sputtered-W-distribution model. For D and W impact we use the fit function from [14]:

$$f_w(E) = \frac{2a^2 E_s E}{(E + E_s)^3}, \quad a \equiv 1 + \frac{(M_1 + M_2)^2}{4M_1 M_2} \frac{E_s}{E_0}. \quad (4)$$

where M_1 and M_2 are the atomic masses of the target and projectile atoms (ions); E_0 and E_s are the surface binding and impinging particle energies. For the C induced W sputtering we use a simple model:

$$f_w(E) = \begin{cases} \text{const}, & \text{for } E \leq E_{\max} = 10 \text{ eV}, \\ 0, & \text{for } E > E_{\max}. \end{cases} \quad (5)$$

The angular distribution for the both models is the ‘‘cosine’’ one: $\cos(\alpha) = \text{Random Number}$, where α is the angle between the velocity on injected W and the normal to the divertor plate.

During the simulation we use 60 000 cells along the poloidal direction. This allows finest resolution in space down to the Debye length and electron gyro-radius. All simulations have been performed on HELIOS supercomputer (Rokkasho, Japan). Each run took in average 20 000 CPU hours on 1024 processors, all together (including test runs) about 300 000 CPU hours have been consumed.

3. SIMULATION RESULTS

During the simulations we adjust the plasma and the heat source parameters to match the experimentally observed upstream SOL density, n_u , and electron temperature, $T_{e,u}$. For reference we consider the Pulse No's: 81472, 81478 and 81484 with $n_u \sim 1.5\text{--}1.8 \times 10^{19} \text{ m}^{-3}$, $T_{e,u} \sim 45\text{--}75\text{eV}$. Under these conditions we made three sets of simulations:

1. High temperature case ($T_{e,u} \sim 65\text{eV}$) with relatively strong heat source;
2. Low temperature case ($T_{e,u} \sim 45\text{eV}$) with 2.5 times weaker heat source;
3. The case as 1. with the additional injection of $\sim 100 \text{ eV C}^{++}$ ions from the particle source.

In this way we simulate influx of hot carbon ions from the pedestal.

Low temperature carbon particles originating from different plasma-facing-components are modelled via injection of C atoms from the divertors with the fixed flux $10^{21} \text{ m}^2/\text{s}$. C atoms are assumed to be in thermal equilibrium with Franck-Condon distributed D atoms and have the temperature 2eV .

Typical profiles of density and temperature obtained from the simulation are plotted in Fig.5, indicating low concentration of W particles (in different ionised state). To estimate the concentration of W ions we consider the ‘‘W-related’’ Z-effective:

$$Z_{eff}^W = \frac{\sum_{D,W} z_i^2 n_i}{\sum_{D,W} z_i n_i}, \quad (6)$$

which is plotted in Fig.6. As we see, the concentration of W ions at the distances more than 1 cm from the divertor plates is negligibly small. Moreover, with the given resolution, $n_{min} \sim 10^{15} \text{ m}^{-3}$, we do not observe W ions with ionization state more than 4.

These results can be explained after analyzing of divertor plasma parameters from the Table 1. As we can see, that with increasing upstream temperature increases potential drop across the divertor plasma. As a result the electric field towards the divertor increases too and more W ions are attracted back to the plates (cf. the cases 1 and 2). Simulations also indicate that cross- field diffusion of W ions and loss of W atoms at the radial boundaries are negligibly small: the total number of W particles crossing the radial is less that 0.1% of W ions redeposited at the divertors. In other words, the majority of the W is ionized are ‘‘promptly redeposited’’ to the divertor plates (see Fig.6). There is no significant contribution of hot C^{++} ions originating from the upstream SOL, because they are cooled down before reaching the divertor plasma. The consequence of the low W concentration is relatively high electron temperature (they are not cooled enough) and low density at the divertors obtained in the simulation.

CONCLUSIONS

Our simulations indicate that with the given tungsten sputtering data it is impossible to reproduce the experimentally observed W radiation in the SOL (e.g. see [15]). For low temperature plasmas the energy of D and C ions hitting to the divertor plates is too low to sputter sufficient amount of W. With increasing energy the W sputtering increases, but the potential drop in the divertor plasma increases too. As a result, most of the W atoms are ionized in the vicinity of the divertor and return back to the plates. There are two effects leading to the observed redeposition of W ions: first is the “near-divertor” ionization of W due to low ionization potential – 7.86eV (for comparison the ionization potentials for D and C are 13,6 and 10.6eV), second, W_{+n} ions have large Larmor radius $\sim 2/n$ mm, so that they are promptly redeposited.

Possible explanations of these results are the following: under realistic conditions the threshold energies for W sputtering are significantly lower than ones given in literature; the radial electric field, which is not taken into account in present model, can also contribute to increasing of the effective W sputtering; there is a strong self-sputtering of W ions in highly ionized state, which are penetrating into the SOL from the pedestal, propagate towards the divertors and accelerating above the threshold energies in the divertor sheath. These points will be addressed in our future work.

ACKNOWLEDGEMENTS.

This work was supported by EURATOM and carried out within the framework of the European Fusion Development Agreement. The views and opinions expressed herein do not necessarily reflect those of the European Commission. We thank D. Coster for useful discussions. The first author acknowledges support by the projects P21941-N16 and GNSF/ST09_305_4-140.

REFERENCES

- [1]. D. Tskhakaya, S. Jachmich, et al., Journal of Nuclear Materials, **415** (1), (2011) S860.
- [2]. D.P. Coster, Journal of Nuclear Materials, **415** (1), (2011) S545.
- [3]. T. Takizuka, K. Shimizu, et al., Nucl. Fusion, **49**, (2009) 075038.
- [4]. E. Havlickova, W. Fundamenski, et al., Plasma Physics and Controlled Fusion, **54**, (2012) 045002.
- [5]. D. Tskhakaya, Cont. Plasma Phys., to be published (2012).
- [6]. S.I. Braginskii, Transport processes in a plasma, in: M.A. Leontovich (Ed.), Reviews of Plasma Physics, vol. 1, Consultants Bureau, New York, 1965.
- [7]. A. F. Alexandrov, L. S. Bogdankevich, A. A. Rukhadze, Principles of Plasma Electrodynamics, Springer-Verlag. Berlin, Heidelberg, New York, Tokio. 1984.
- [8]. D. Tskhakaya, A. Sobba, et. al., proceedings of 18th Euromicro Conference on Parallel, Distributed and Network-based Processing, Pisa Italy, IEEE, 2010, 476.
- [9]. J. Bohdansky, Nuclear Fusion, Special issue, (1984), p.61.
- [10]. W. Eckstein, Top. Applied Physics papers, **110**, (2007) 33; Vacuum, **82**, (2008) 930.

- [11]. M. Stenke, K. Aichele, et al., Journal of Physics B: Atomic Molecular Optical Physics **28**, (1995) 2711, 4853.
- [12]. L. Vainshtein, I. Beigman, et al., Journal of Physics B: Atomic Molecular Optical Physics, **44**, (2011) 125201.
- [13]. K. Vörtler, C Björkas and K. Nordlund, Journal of Physics: Condensed Matter **23**, (2011) 085002.
- [14]. W. Eckstein, IPP report, IPP 9/132, (2002).
- [15]. G.J. van Rooij, this conference.

Case/Value	1	2	3
$n_e \times 10^{19} m^{-3}$	4.5, 3.3	3.4, 3.5	3.2, 2.9
$T_e eV$	37, 53	20, 38	47, 58,
$\Delta\phi V$	145, 176	88, 132	175, 188
$F_W^{div} \times 10^{20} m^2 / s$	5.9, 3.5	5.1, 3.1	3.3, 3.8

Table 1: Plasma parameters at the divertors. First and second values correspond to the inner and outer divertors, respectively. F_W^{div} and $\Delta\phi$ denote the W ion flux density to the divertor plates and the potential drop across the divertor plasma.

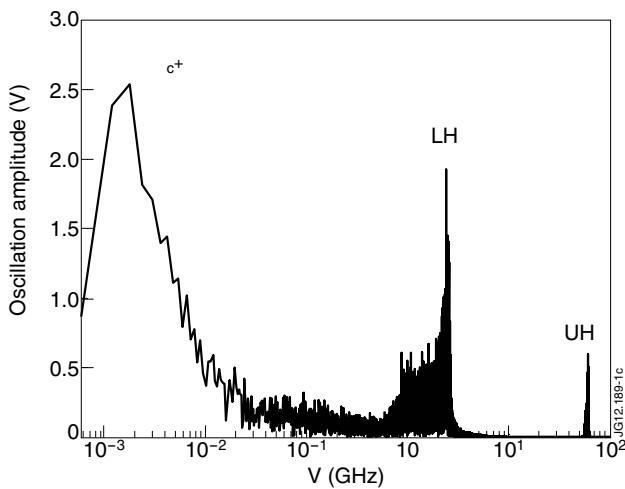


Figure 1: Potential oscillation spectrum at the magnetic presheath entrance in the outer divertor plasma.

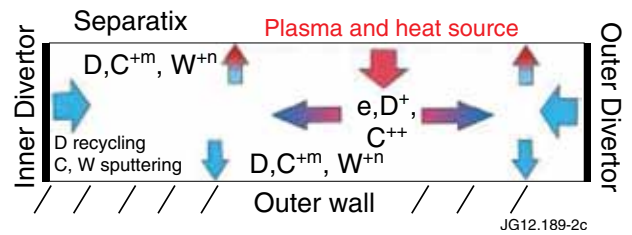


Figure 2: PIC simulation geometry.

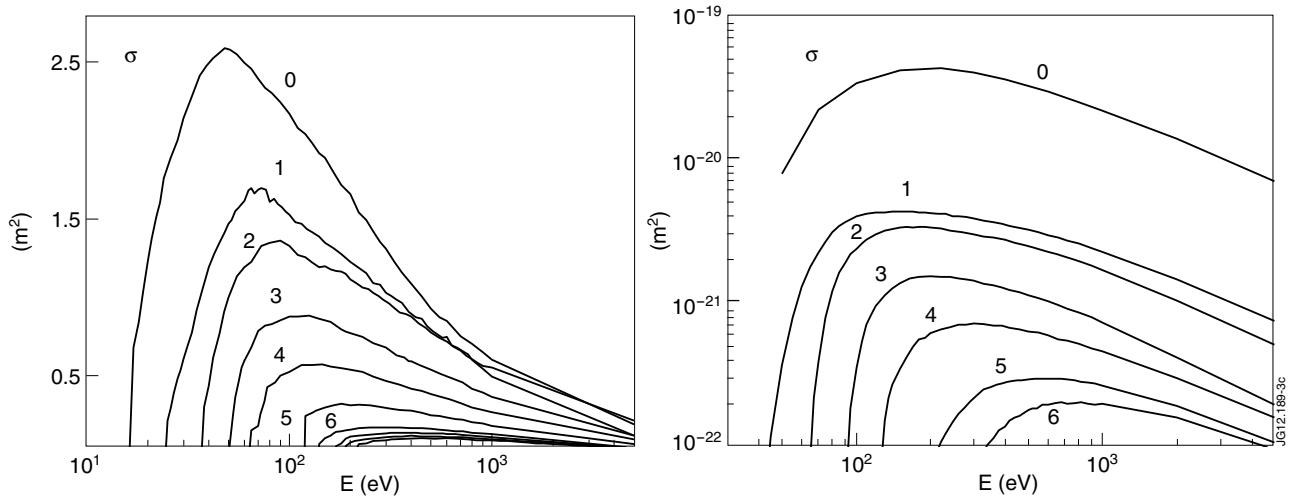


Figure 3: Single (a) and double (b) electron-impact ionization cross-sections for tungsten implemented in the BIT1 code. Numbers indicate initial ionization state.

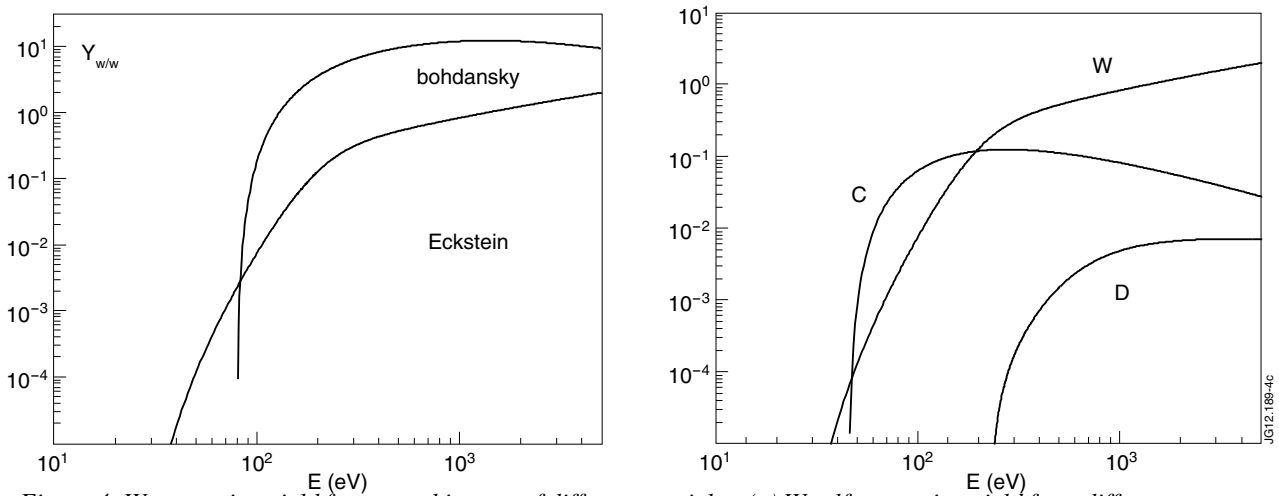


Figure 4: W-sputtering yield for normal impact of different particles. (a) W self-sputtering yield from different sources; (b) yields implemented in the BIT1 code.

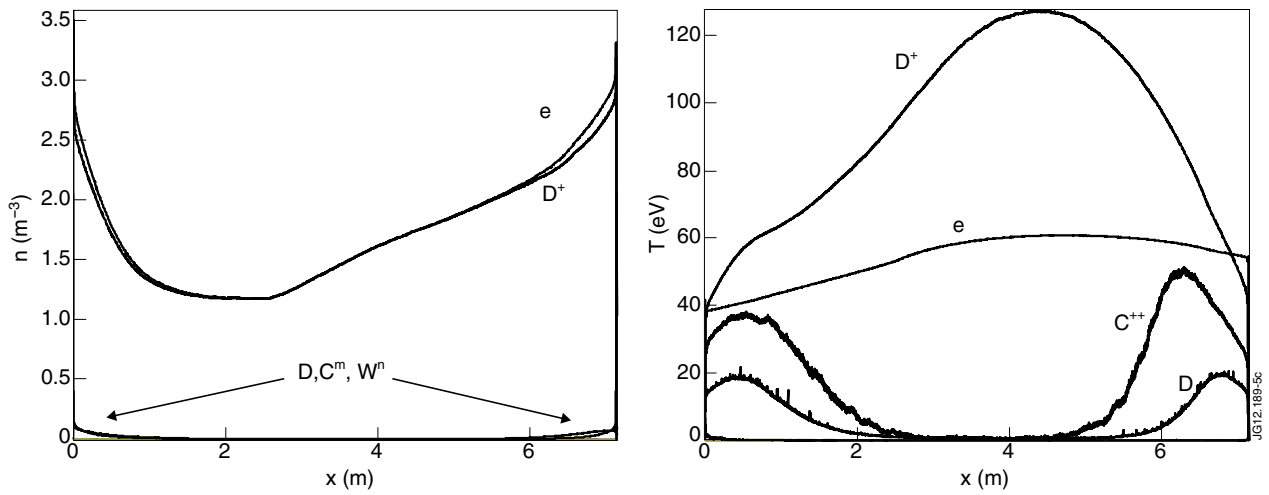


Figure 5: Poloidal profiles of the density (a) and the temperature (b) in the SOL for the case 1.

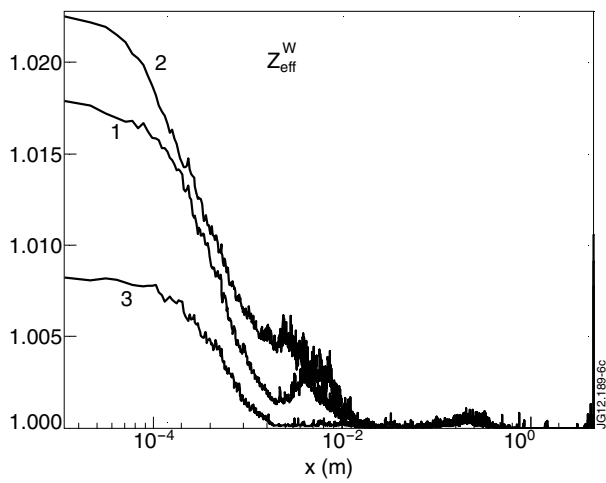


Figure 6: Poloidal profiles of W_{eff}^Z . The numbers “1”, “2” and “3” denote the simulated case.